journal

J. Am. Ceram. Soc., **99** [6] 2040–2046 (2016)
DOI: 10.1111/jace.14097

High-Temperature Multilayer Ceramic Capacitors Based on $100-x(94Bi_{1/2}Na_{1/2}TiO_3–6BaTiO_3)–xK_{0.5}Na_{0.5}NbO_3$

Claudia Groh,[‡] Keisuke Kobayashi,[§] Hiroyuki Shimizu,[§] Yutaka Doshida,[§] Youichi Mizuno,[§] Eric A. Patterson,[‡,†] and Jürgen Rödel[‡]

[‡]Institute of Materials Science, Technische Universität Darmstadt, Darmstadt 64287, Germany

[§]Materials R&D Department, R&D Laboratory, Taiyo Yuden Company, Ltd., Takasaki, Gunma, Japan

The potential high-temperature dielectric materials $100-x(94Bi_{1/2}Na_{1/2}TiO_3–6BaTiO_3)–xK_{0.5}Na_{0.5}NbO_3$ with $x = 12$, 18, and 24 were processed as bulk samples in order to examine the reduction of sintering temperature by means of CuO as sintering aid. Due to the successful reduction of sintering temperature, low cost Ag:Pd could be used as a co-fired electrode material for multilayer ceramic capacitors (MLCCs). Fabrication of 8 μm thick, dense MLCCs with self-contained, nonreactive electrodes is reported for a wide range of compositions of $Bi_{1/2}Na_{1/2}TiO_3–BaTiO_3–K_{0.5}Na_{0.5}NbO_3$. Among the manufactured MLCCs, those with compositions $x = 24$ showed the most promising dielectric properties for applications where high operating temperatures are needed. The temperature-dependence of permittivity was quite low, revealing a change of less than ±10% compared to its 150°C-value in the range of 40°C–225°C. For samples sintered at 1000°C, an RC constant of about 300 s was obtained at 150°C. Furthermore, these $x = 24$ MLCCs exhibited the finest microstructures among the compositions examined; making it a suitable candidate for further miniaturization of layer thickness as required for state-of-the art devices.

I. Introduction

The market of ceramic capacitors is growing steadily largely due to the large variety of applications for passive components in electronic devices.[1] At the same time, the demands on state-of-the art electronic devices are increasing rapidly; among the important characteristics are miniaturization, low-cost production, frequency- and temperature-stability and high reliability.

The development of SiC-based power devices (such as JFET, MOSFET, high-voltage switching devices) will open up a new application field for electronics, especially for automotive applications.[2,3] By considering drift region conductivity, it was found that 6H–SiC devices should only become fully intrinsic at temperatures greater than 1000°C. Calculations showed theoretical operation of Schottky rectifiers and MOSFET devices is possible at temperatures up to 600°C.[4] Other work demonstrated that SiC is at least capable of operating at 227°C for MOSFETs and Schottky rectifiers.[5] Since the temperature of SiC devices can reach up to 300°C in an engine, passive devices used with any SiC circuit are also required to withstand the same harsh environments. Multilayer ceramic capacitors (MLCCs), which would necessarily be used in close conjunction with SiC semiconductor devices, are a key passive component needed to realize functional high-temperature SiC devices.

The most widely used materials for commercial MLCCs are ferroelectrics based on modifications in the composition of $BaTiO_3$ (BT), however, its relatively low Curie temperature (T_c) of about 130°C limits its high-temperature applications.[6–8] The formation of MLCCs comprised of market dominating $BaTiO_3$ has been studied for many years, resulting in a steady improvement of properties.[9,10] Although some efforts have been made to increase the Curie temperature, the upper limit achieved is still below 200°C, which is too low for the type of high-temperature applications of interest.[11] There are some commercial high-temperature-MLCCs made with paraelectric materials stable to 200°C (Kemet High-Temperature C0G series). These devices have smaller temperature coefficients of capacitance because they do not experience phase transition between operating temperature, however, the magnitude of the permittivity is relatively small.

Recently, a variety of material systems has shown promise as high-temperature dielectrics, including various binary systems like $CaZrO_3$ or Nb_2O_5-doped BT-$(Bi_{1/2}Na_{1/2})TiO_3$ (BT-BNT)[6,12] Mn-doped BNT-$CaTiO_3$ (BNT-CT),[13] BT-$Bi(Zn_{0.5}Ti_{0.5})O_3$ (BT-BZT),[14] and BT-$BiScO_3$ (BT-BS).[15,16] Ternary systems were developed from further modification of these binary systems such as BT-BS-$(Bi_{1/2}K_{1/2})TiO_3$ (BT-BS-BKT),[17] and BNT-BT-$(K_{0.5}Na_{0.5})NbO_3$, (BNT-BT-KNN),[18] BNT-BKT-KNN,[19] BT-BZT-BS,[20], and BT-BZT-$BiInO_3$ (BT-BZT-BI).[21] This work will focus on the benefits of higher solubility of KNN into BNT-BT-KNN, using larger amounts of KNN content relative to previous studies.

One of the major challenges for advancing these ceramics into real applications is their successful implementation into MLCCs, which is necessary to enhance the volumetric efficiency, compared to bulk samples.[1] Several of these binary and ternary solid solutions were first developed as lead free piezoelectric alternatives. In some of these systems, multilayer actuator devices have been made but were focused on compositions where temperature stable permittivity was not considered. For example, devices have been manufactured for stack actuator applications using lead-free piezoelectric in systems such as BNT, BNT-BT, and BNT-BT-KNN.[22,23] Out of the recently reported high-temperature dielectrics BT-BZT-BS, the properties were shown to match the bulk characteristics when made into multilayer components.[20] However, for most of the other systems, the development of MLCCs is largely lacking.

It is known from $BaTiO_3$-based MLCCs, that the choice of materials utilized to form inner electrodes has a remarkable influence on the total cost and stability of the MLCCs produced.[8] Typically for prototype devices, internal electrodes are formed by precious metals such as platinum or palladium, which can easily be co-fired up to at least 1300°C

J. Ihlefeld—contributing editor

Manuscript No. 37092. Received June 23, 2015; approved December 1, 2015.
[†]Author to whom correspondence should be addressed. e-mail: pattersn@ceramics.tu-darmstadt.de

in air atmosphere. Since precious metals are usually comparably stable against interdiffusion with the ceramic layers, this allows an easier materials design in the MLCCs to demonstrate their properties. A severe reduction of cost for internal electrodes can be achieved by utilizing Ag:Pd alloy (e.g., Ag:Pd = 70:30), since the cost of silver is more than 20 times smaller than that of palladium. However, this limits the sintering temperature of MLCCs, since the melting temperature of the electrode materials decreases with increasing silver content.[24] Previously, when high temperatures were used, Pd was shown to react with Pb and Bi-based oxides, so precautions should be taken in their implementation to prevent secondary phase formation and related deterioration of electrical properties.[25,26] Thus, it is often useful for the sintering temperature of the dielectric material itself to be reduced. In early work by Hennings, the sintering temperature of BT was shown to be reduced when CuO was added to form a liquid phase at 1070°C.[27] It was also observed that reacting with TiO_2, the CuO can form a liquid phase of Cu_3TiO_4 at 1000°C.[27] Due to the higher rate diffusion of the perovskite in the liquid phase, the rate of densification and, at longer sintering times, grain growth can be improved. In certain lead-free piezoceramics, sintering aids such as CuO for BNT-$BaZrO_3$,[28] KNN[29,30] BNT-BT,[31] and BNT-BT-KNN[32] are known to reduce the sintering temperature and to improve the density. For CuO added to KNN, a secondary phase of K_4CuNb_8O[23] forms and melts at 1050°C.[29,30] In KNN-5BT samples with CuO added was shown to create dense samples when sintered at 950°C and a liquid phase was also observed and preliminarily suggested to be due to BaO–CuO, but no confirmation of the composition of this phase was obtained.[33] In the case of 92BNT-6BT-2KNN samples, closely related to the compositions of this work, doping with 1 mol% CuO was likewise shown to lower the sintering temperature to 950°C (with >98% relative density), although the exact nature of the liquid phase was again not determined.[32]

For this study, the primary objective was to manufacture Ag/Pd inner electrode MLCCs made of the $100-x(94Bi_{1/2}Na_{1/2}TiO_3\text{-}6BaTiO_3)\text{-}x(K_{0.5}Na_{0.5}NbO_3)$ system, one of the previously described promising high-temperature dielectric materials. Within this objective, three main goals were explored by this work. First, lowering the sintering temperature of the bulk material by using CuO as a sintering additive was attempted. Next, the effects of KNN content and CuO-additive on the dielectric properties, especially temperature-dependent permittivity behavior, were characterized. Finally, MLCCs were fabricated and the effect of the Ag/Pd inner electrodes was investigated.

II. Experimental Procedure

(1) Powder Synthesis

Ceramic powders of compositions $100-x(94Bi_{1/2}Na_{1/2}TiO_3\text{-}6BaTiO_3)\text{-}x(K_{0.5}Na_{0.5}NbO_3)$ for x = 12, 18, and 24 (hereafter labeled 12KNN, 18KNN, and 24KNN) were produced by means of mixed oxide route using commercially available powders of Bi_2O_3 (98.5%), $NaCO_3$ (99.8%), $BaCO_3$ (99.5%), TiO_2 (99.9%), K_2CO_3 (99.5%), and Nb_2O_5 (99.5%) purity. These constituents were mixed for 24 h in an ethanol slurry, using zirconia balls as milling media. The resulting powders were calcined at 900°C for 3 h in air atmosphere with a 5°C/min heating rate. The XRD patterns of the calcined powders of 12KNN, 18KNN, and 24KNN reveal perovskite-type structures with no second phases present.

(2) Synthesis of Bulk Samples

Bulk samples were prepared in order to (i) allow a comparison of the properties of bulk samples to those of MLCCs to evaluate the effect of MLCC-processing and (ii) in order to assess the ability of CuO to reduce the sintering temperature. Therefore, two types of powders were produced. First, reference stoichiometric powders without additives (labeled xKNN) and secondly, the same composition powders with 1 mol% CuO (xKNN:Cu) added. After a second identical milling step, the powders were uniaxially pressed into 10 mm diameter pellets. A sintering study at various temperatures in the range between 960°C and 1100°C for 3 h was conducted with a 3°C/min heating rate. The relative densities of bulk samples sintered at various temperatures were measured by Archimedes method and comparison to the theoretical densities. The theoretical densities were determined by means of whole pattern fitting of the pseudo-cubic XRD patterns. Afterwards, a silver electrode was formed by burning in silver paste.

(3) Synthesis of MLCCs

MLCCs comprised of xKNN:Cu with x = 12, 18 and 24 were produced. The powders were mixed with a poly vinyl butyral (PVB)-based binder in order to prepare the respective tape casting slurries. These slurries were utilized to form green-sheets via the doctor-blade method. In order to form inner electrodes Ag:Pd (70:30) paste was printed on the green-sheet by a screen printing method. The MLCCs comprised 10 active layers. In order to perform a sintering study similar to the bulk one, the green-body MLCCs were sintered at different temperatures in 40°C steps in the range between 920°C and 1040°C for 2 h, again with a 3°C/min heating rate. The surface area of the final MLCCs was 2.9 mm × 1.0 mm. The resulting active dielectric layers were 8 μm in thickness.

(4) Characterization

The microstructure was observed by Scanning Electron Microscopy (SEM S4300; Hitachi High-Tech Fielding Corporation, Tokyo, Japan) and elemental distributions were detected by Energy Dispersive X-ray (EDX) Spectroscopy. The temperature-dependent permittivity and loss was determined at 1 kHz. At high temperatures (T = 40°C–400°C) an LCR meter (HP 4192A; Agilent Technologies, Santa Clara, CA) and an attached high-temperature oven (D900 series; Despatch Industries, Minneapolis, MN) was utilized. For the low temperature permittivity measurements (T = −55°C to 160°C), an LCR meter (E4980A; Agilent Technologies) was

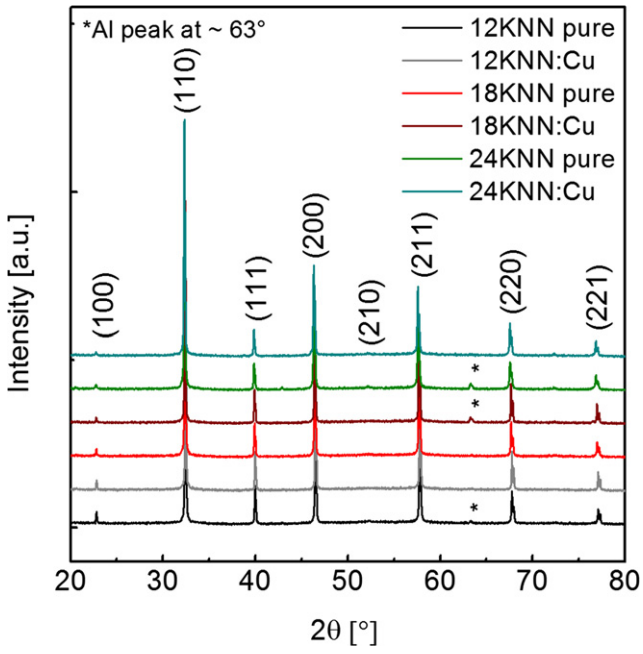

Fig. 1. XRD patterns displaying pseudo-cubic perovskite structure for bulk samples shown for 12, 18 and 24KNN with and without Cu, as sintered at 1100°C.

used, and the samples were cooled by means of liquid nitrogen in the same type of temperature chamber as before. The RC constants at 150°C were calculated using the resistance at 40.8 V and the capacitance determined at 1 V.

III. Results and Discussion

(1) Bulk Samples

The XRD patterns of all calcined powders reveal second phase-free perovskite-type structures. Furthermore, as displayed in Fig. 1, XRD on bulk sintered samples also revealed pseudocubic perovskite-type structure for all *x*KNN at 1100°C. These results were characteristic for all other sintering temperatures evaluated. For some of the bulk samples, small additional peaks at around 43° and 63° were present. Upon further investigation, these were found to correlate with the aluminum sample holder used to mount the sintered samples in the XRD and can thus be disregarded.

The relative densities of *x*KNN and *x*KNN:Cu with $x = 12$, 18 and 24 are displayed in Fig. 2. The pure xKNN samples can be successfully sintered only at 1100°C, achieving densities in the range of 93%–95%. However, reducing the sintering temperature to 1040°C results in a severe drop in densities to <85%, which is too low for using these materials in dielectric devices.

The densities of *x*KNN:Cu are enhanced over a broad range of sintering temperatures compared to the pure *x*KNN. This implies that CuO is effective in reducing the sintering temperature. The densities for all *x*KNN:Cu samples were above 95% for sintering temperatures between 1000°C–1100°C. At 960°C, the densities are significantly reduced to 92%, which is comparable to the best of the pure *x*KNN samples sintered at 1100°C.

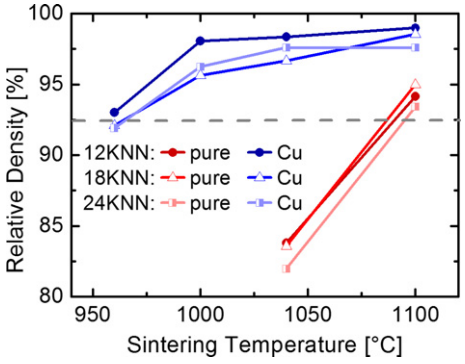

Fig. 2. Relative densities of *x*KNN and *x*KNN:Cu with $x = 12$, 18 and 24, respectively, at various sintering temperatures.

The microstructure of *x*KNN and *x*KNN:Cu bulk samples sintered at 1100°C was investigated by means of SEM, as illustrated in Fig. 3. The bulk samples of *x*KNN sintered at 1100°C reveal a dense microstructure with grain sizes in the range of 0.1–0.5 μm. In contrast, for *x*KNN:Cu larger grain sizes compared to the pure *x*KNN system were obtained which suggests that the sintering additive modifies the sintering behavior. Within the *x*KNN:Cu system, the grain size roughly decreased from 2 to 0.5 μm as *x*KNN content increased from 12KNN to 24KNN, respectively. While CuO is added in this case as a sintering aid, it also is soluble on the B-site of KNN as a dopant and has been shown to simultaneously increase density and decrease grain size of pure KNN.[34] Thus, as *x*KNN is increased, the decreasing grain size could be explained by less of the Cu remaining at the grain boundaries to act as a liquid phase sintering aid as it is instead incorporated more easily into the structure of the solid solution.

Thus, when processing *x*KNN with the help of a constant amount of CuO sintering additive necessary for producing co-fired MLCCs, it must be noted that the content of *x*KNN:Cu plays an important role in the final grain size. For application in MLCCs, it is necessary to form small grains in order to be able to realize thin-layered-MLCCs to follow the general trend of miniaturization of devices.[1] Furthermore, small grains are important to maintain a good reliability under high voltage use.

Figure 4 depicts the temperature-dependent permittivity curves of nominally pure 12, 18 and 24KNN sintered at 1100°C. They reveal that the maximum in permittivity decreases and shifts to lower temperatures with increasing *x*KNN content, namely from $\varepsilon_r = 3490$ at 155°C (12KNN), to $\varepsilon_r = 3110$ at 125°C (18KNN), to $\varepsilon_r = 2670$°C at 105°C (24KNN). This results in a desired flattening of the curve with increasing *x*KNN content. On the other hand, the permittivity at each specific temperature is decreasing with increasing *x*KNN content. This behavior is in very good agreement with the temperature-dependent permittivity curves of the same system previously reported.[18]

The temperature-dependent permittivity and loss curves of *x*KNN:Cu sintered at various temperatures are displayed in

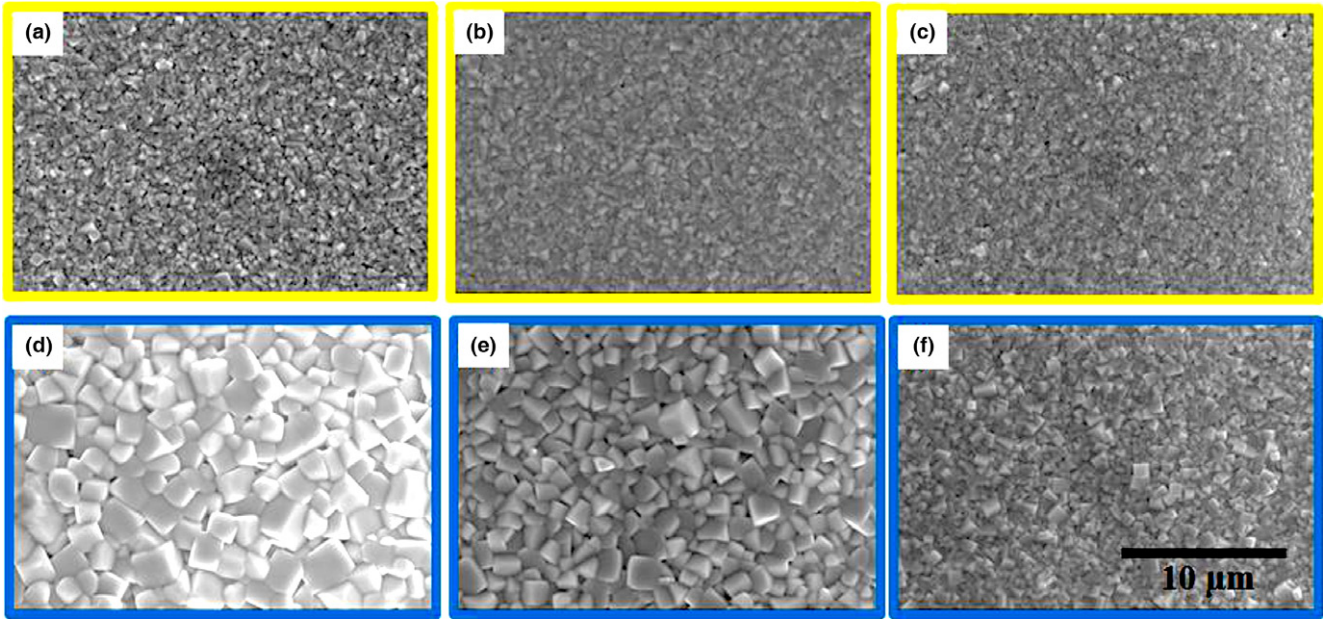

Fig. 3. SEM images of bulk samples sintered at 1100°C for (a), (b) and (c) 12KNN, 18KNN and 24KNN without CuO sintering additive and (d), (e) and (f) 12KNN:Cu, 18KNN:Cu and 24KNN:Cu, respectively.

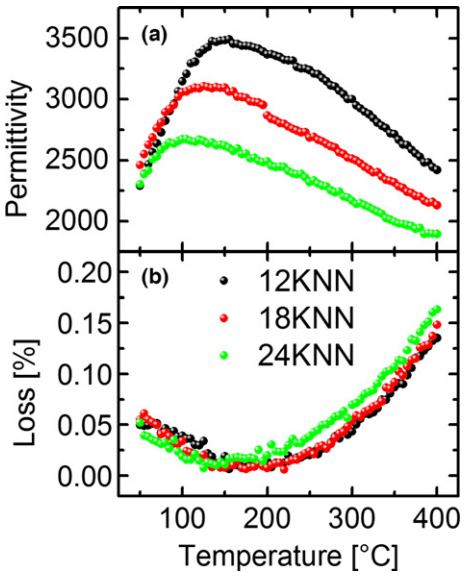

Fig. 4. Temperature-dependent permittivity (a) and loss (b) of pure xKNN bulk samples sintered at 1100°C with $x = 12$, 18, and 24, respectively (at 1 kHz).

Fig. 5. The characteristic features found for pure *x*KNN are captured in the same range of the *x*KNN:Cu system. For each *x*KNN composition sintered between 1000°C and 1100°C, the sintering temperature had only a minor effect on the temperature-dependent permittivity curves, which seems reasonable considering the correspondingly small variation of density in this range. The temperature-dependent loss at higher temperatures is increased with decreasing sintering temperature, especially for 18KNN:Cu and 24KNN:Cu at 960°C. This is most likely due to the decrease in density seen at lowered sintering temperatures.

By utilizing CuO as sintering additive, the permittivity is increased in comparison to the respective pure *x*KNN samples. Samples sintered at 1100°C were used for this comparison because for sintering temperatures of 1040°C or below, *x*KNN without CuO had denisities of less than 85% and were not suitable for permittivity measurements. Increases in maximum ε_r were found to be 1000, 400, and 500 for 12KNN, 18KNN, and 24KNN, respectively, when CuO was added. This suggests that the improved densification due to the Cu sintering additive also benefitted the dielectric properties. The best temperature stability of permittivity was achieved for 24KNN:Cu. Additionally, the microstructure of 24KNN:Cu was, compared to 12KNN:Cu and 18KNN:Cu, much finer which is advantageous for forming MLCCs with very thin layers required for miniaturization of electrical components.

With the inclusion of sintering additives, the sintering temperature at which dense bulk samples are formed was reduced below the target temperature (1040°C) for using Ag:Pd inner electrodes. Therefore, the following section of MLCC results focuses on samples sintered at 1040°C or below. The dielectric properties of 1000°C are emphasized in particular.

(2) MLCCs

The successful formation of MLCCs is revealed by cross-sectional microstructure, representatively provided for 24KNN:Cu sintered at 1040°C in Fig. 6. Minor defects in the electrodes and some defects at the interface between the electrode and the ceramic layer, as well as in the ceramic layer were observed. A sharp interface between the Ag:Pd inner electrodes and the ceramics layers, however, was

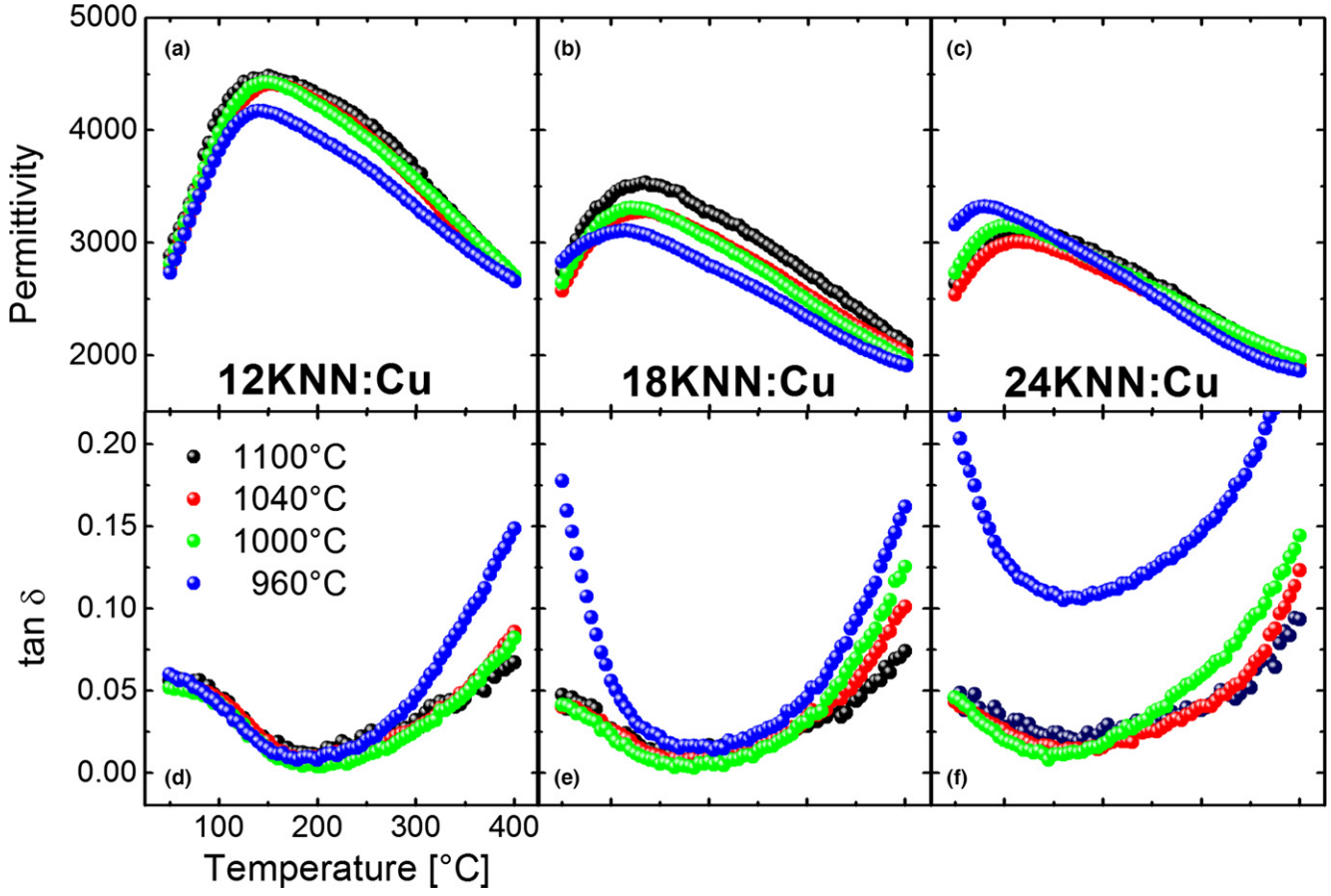

Fig. 5. Temperature-dependent (a), (b), (c) permittivity and (d), (e) (f) loss for xKNN:Cu bulk samples (at 1 kHz) sintered at various temperatures with $x = 12$, 18 and 24, respectively.

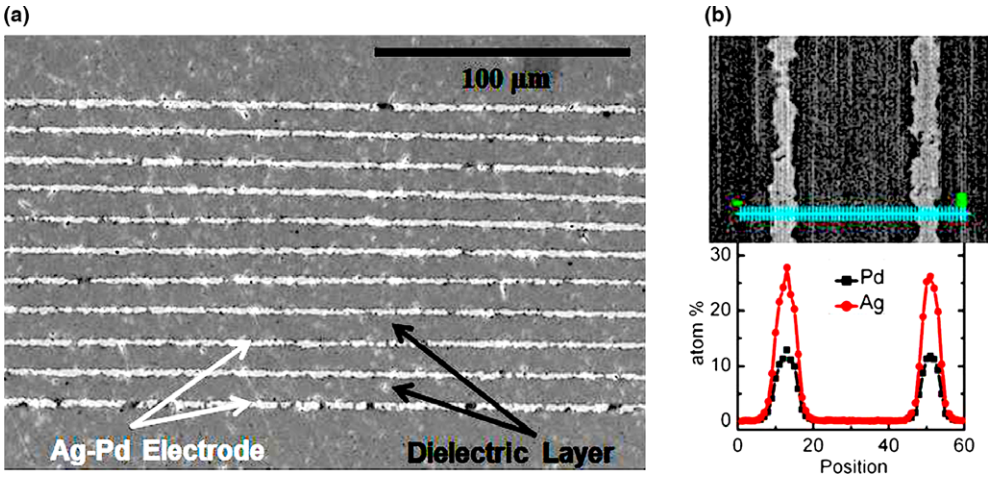

Fig. 6. Cross-sectional microstructure of MLCCs of 24KNN:Cu sintered at 1040°C displaying (a) 10 active ceramics layers with internal Ag:Pd electrodes and cover layers at the bottom and top of the MLCC and (b) EDX analysis performed across two internal electrodes confirming the successful formation of self-contained internal Ag:Pd electrodes.

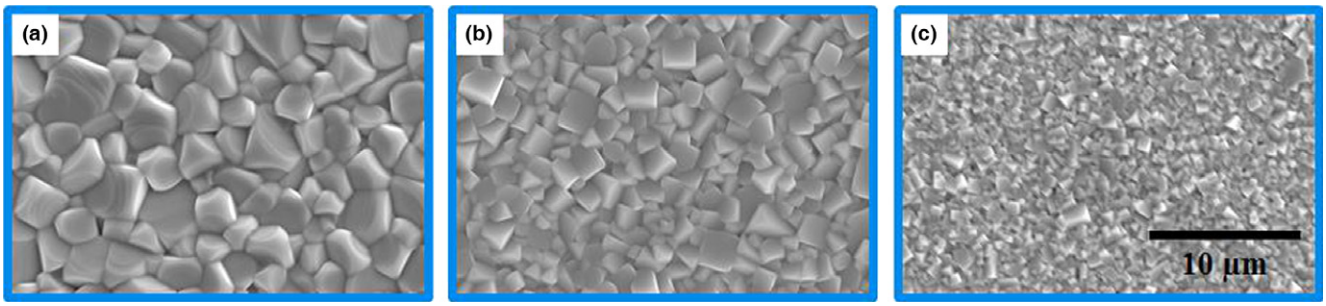

Fig. 7. Comparison of the microstructures of MLCCs comprised of *x*KNN:Cu with $x = 12$ (a), 18 (b) and 24 (c) sintered at 1000°C.

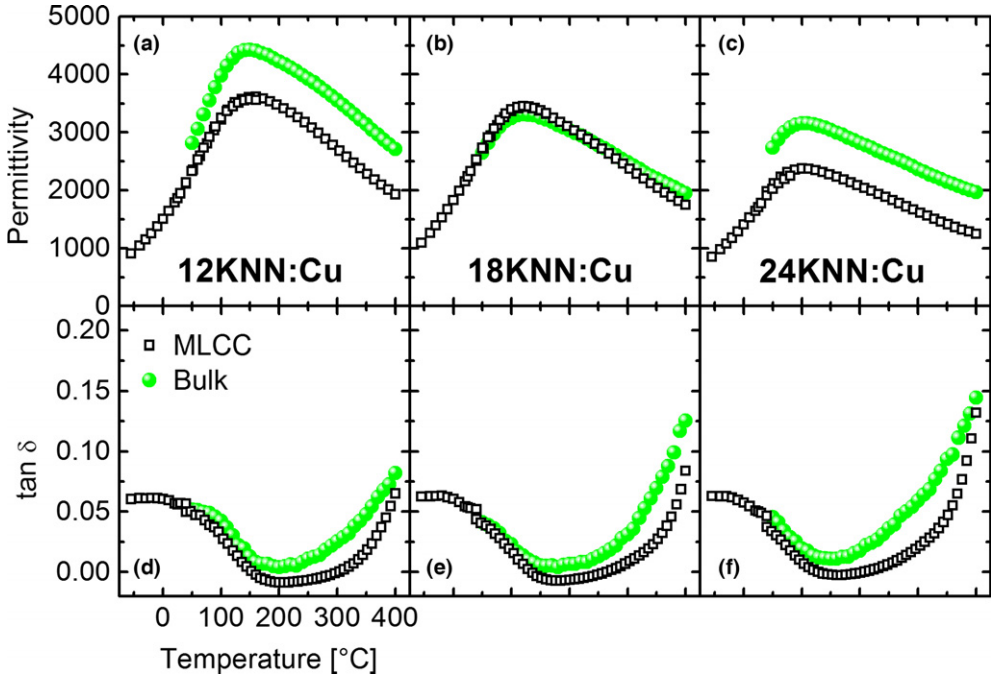

Fig. 8. Comparison of temperature-dependent 1 kHz permittivity (a), (b), (c) and loss tangent curves (d), (e), (f), of both MLCCs and bulk samples comprised of xKNN:Cu with $x = 12$, 18 and 24, respectively. A slight jump in the loss data shows where the separate high and low temperature measurements were combined in the image. All samples shown were sintered at 1000°C.

observed in cross-sectional SEM images. In the case of 24KNN:Cu MLCCs, no interdiffusion between the electrode and ceramic layers was detectable (up to a sintering temperature of 1040°C) within the resolution limit of the EDX measurement (~0.5 at.%) used in this study [Fig. 6(b)].

Figure 7 presents the microstructures of the MLCCs comprised of *x*KNN:Cu with $x = 12$, 18 and 24 sintered at 1000°C. This confirms that with increasing *x*KNN content for *x*KNN:Cu MLCCs, the trend of decreasing grain size is the same as observed in the bulk samples. This similarity

between the bulk samples and MLCCs suggest that there is no severe change in sintering behavior while co-firing the MLCCs with Ag:Pd inner electrodes.

Figure 8 provides a comparison of temperature-dependent permittivity and loss curves of both bulk samples and MLCCs comprised of xKNN:Cu with x = 12, 18 and 24, all sintered at 1000°C. The behavior of the temperature-dependent permittivity curves of MLCCs reflects the ones of the bulk samples, i.e., the curves flatten out with increasing xKNN content.

Interestingly, the shapes of the MLCC-curves resembled those of the bulk samples, however, the absolute permittivity values for 12KNN:Cu and 24KNN:Cu MLCCs were lower compared to their respective bulk samples. This suggests that the overall properties of the bulk samples were maintained while forming the MLCCs, i.e., there has been no severe interdiffusion or phase change in the xKNN:Cu. The decrease of absolute permittivity in 12KNN:Cu and 24KNN:Cu could be due to a reduction of the active area in the MLCCs. This can arise from processing issues such as shifting of electrodes in the MLCCs during stacking, scattered discontinuities in the electrode layers, or insufficient connection of active layers to electrode layers. Apart from that, even though no severe microstructure change is apparent at the first glance when comparing bulk samples and MLCCs, the sintering conditions are influenced in various ways. At low temperatures, the permittivities of all MLCCs decrease continuously with no further apparent anomaly. Interestingly, the permittivity at −55°C is nearly independent of the xKNN content with values in the range of about 1000.

The temperature coefficient of the permittivity, TCε, at 300°C was calculated within the approximately linear region of the 1 kHz dielectric data (between 200°C and 400°C). All compositions were calculated for both the bulk and MLCC samples and were found to have a negative value in all instances, as seen in Table I. While there was not a large change between 12 and 18KNN:Cu samples, at 24KNN:Cu, the TCε of the bulk samples revealed a large drop. For the MLCC samples, the values were higher in all cases. The overall decrease in TCε from 12KNN:Cu to 24KNN:Cu samples was almost the same (~300 ppm/°C) for both the bulk and MLCC samples.

In most applications the **E**lectronic **I**ndustries **A**lliance (EIA) standard EIA RS-198- Code is normally used to classify the type of ceramic capacitor. Here, a lower and upper temperature and a capacity change are given for each type. For high-temperature applications, however, there is no suitable standard currently in place, since most MLCCs are usually classified up to a maximum temperature of 200°C. Also, the classifications available regarding MLCCs are judged by the changes of permittivity at 25°C, which is reasonable for standard applications. However, for high-temperature application, it is more suitable to derive the temperature stability in relation to an elevated temperature, such as 150°C.

The change in capacitance of the most promising MLCC composition (24KNN:Cu) in reference to 150°C is presented in Fig. 9, revealing that between 40°C and 225°C a deviation of capacitance smaller than ±10% is achieved. Extending this deviation to ±20% yields a temperature range from 30°C to 275°C.

Table I. Temperature Coefficient of Permittivity at 300°C for xKNN:Cu with x = 12, 18, and 24 Derived from 1 kHz Dielectric Data in Fig. 8.

	Bulk TCε [ppm/°C]	MLCC TCε [ppm/°C]
12KNN	−2134	−2807
18KNN	−2180	−2773
24KNN	−1797	−2516

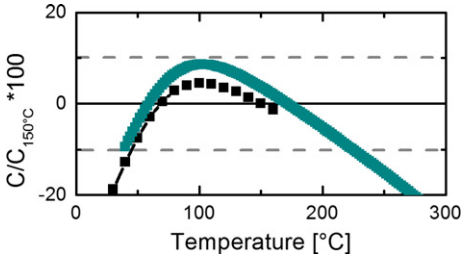

Fig. 9. Change of capacitance at 150°C for 24KNN:Cu MLCCs sintered at 1000°C. The plot contains data from separate high and low temperature measurements. The change of capacitance was calculated based on the capacitance value of the low temperature measurement at 150°C. The dashed gray line represents a change in capacitance of about ±10%.

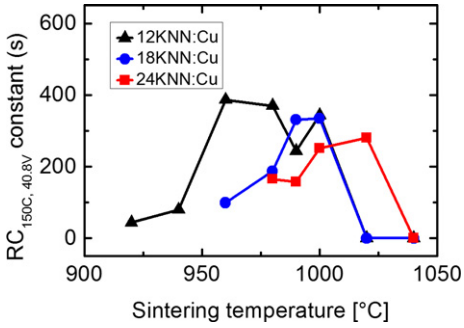

Fig. 10. RC constants of xKNN:Cu MLCCs with x = 12, 18 and 24, respectively, sintered at various temperatures.

Table II. Optimum RC Constants at 150°C for xKNN:Cu and Resistivity Values Calculated from Observed Resistance Values for x = 12, 18 and 24 as Derived in Fig. 10. Sintering Temperature Used is Indicated Below the Composition.

	12KNN (at 960°C)	18KNN (at 990°C)	24KNN (at 1020°C)
Optimum RC constant	387 s	331 s	280 s
Resistivity	1.14 × 10^{10} Ωm	1.10 × 10^{10} Ωm	1.38 × 10^{10} Ωm
Capacitance	106.0 nF	94.0 nF	63.2 nF

The RC constants for all xKNN:Cu MLCCs were calculated for all compositions for samples sintered between 940°C and 1040°C, as displayed in Fig. 10. They clearly decreased as the sintering temperature was lowered from 1000°C to 960°C, which is consistent with the drop in density and degradation of dielectric properties found in the bulk samples. Thus, the reduction of the RC constant in the MLCCs at lower sintering temperatures was assumed to be a result of poor densification of the ceramics themselves. For these lower sintering temperatures, the corresponding resistivities were at least one order of magnitude lower compared to those samples sintered at the optimized conditions. All of the samples were tested over a wide range of voltages which corresponded to applied fields from 1 to 20 kV/mm. The resistivity values determined here were measured using a voltage of 40.8 V. This translates to an applied field of 5 kV/mm and is similar to testing fields for use as actuators. So while this is a higher field compared to typical capacitor usage it did not affect the observed optimization point of the RC constant as a function of sintering temperature. Furthermore, it demonstrates that the MLCCs formed were electrically robust in terms of resistivity at higher voltages.

The optimum values of the RC constants determined at 150°C decreased with increasing xKNN content, as displayed in Table II. For each of these maximized RC constants, the respective resistivities of the MLCCs were in a similar range ($\sim 1 \times 10^{10}$ Ωm), as also shown in Table II. In contrast, the magnitude of the permittivity for the different xKNN content MLCCs was considerably different, accounting for the trend seen in RC constants. For all compositions, the maximum permittivity was located within a small range of temperatures near 150°C, which made them especially suitable for comparison. Since the 24KNN:Cu exhibited a lower, more stable temperature-dependent permittivity behavior, the absolute values at the peak of RC constant were smaller in comparison to the other xKNN:Cu samples. A future study over the entire temperature range would be of great interest to see the development of RC constants as a function of temperature.

IV. Conclusions

Investigations on $100-x(94Bi_{1/2}Na_{1/2}TiO_3\text{-}6BaTiO_3)$-$xK_{0.5}Na_{0.5}NbO_3$ bulk samples with x = 12, 18 and 24 suggest that (i) the materials show promising high-temperature dielectric properties and (ii) by means of sintering additives a sufficient reduction of sintering temperature, required for the implementation of low-cost Ag:Pd, has been achieved.

Among the investigated bulk samples, the best temperature stability of permittivity and at the same time finest microstructure was achieved for $76(94Bi_{1/2}Na_{1/2}TiO_3\text{-}6BaTiO_3)\text{-}24K_{0.5}Na_{0.5}NbO_3$ with 1 mol% CuO sintering additive. Both of these features are advantageous for forming MLCCs with thin layers required for future miniaturization of electrical components. By means of CuO sintering additive, the temperature at which dense bulk samples are formed was reduced below the target temperature for utilization of Ag:Pd inner electrodes (<1040°C) for MLCCs production.

The successful formation of high-temperature dielectric MLCCs composed of BNT-based materials was reported. The MLCCs were made with Ag:Pd (70-30) inner electrodes and the promising properties of the bulk ceramics could be maintained in the MLCCs. Among the investigated MLCCs, 24KNN:Cu was considered as the most promising for high-temperature dielectric applications. It reveals the finest microstructure, which is important when considering the miniaturization of electronic equipment, where a reduction of MLCCs size and therefore increasingly thinner ceramic layers are desirable. Furthermore, a relatively temperature insensitive permittivity has been obtained, revealing in the range of 40°C–225°C a change of lower than ±10% compared to its 150°C value. The values of TCε were found to be lowest for 24KNN:Cu with −1797 ppm/°C and −2516 ppm/°C for bulk and MLCC components, respectively. For 24KNN:Cu sintered at 1000°C, a RC constant of about 300 s was achieved at 150°C.

Acknowledgments

CG thanks the State Center AdRIA and EAP the Deutsche Forschungsgemeinschaft (DFG) under project number RO 954/24.

References

[1]H. Kishi, Y. Mizuno, and H. Chazono, "Base-Metal Electrode-Multilayer Ceramic Capacitors: Past, Present and Future Perspectives," *Jpn. J. Appl. Phys.*, **42** [1R] 1–15 (2003).

[2]C. I. Harris, S. Savage, A. Konstantinov, M. Bakowski, and P. Ericsson, "Progress Towards SiC Products," *Appl. Surf. Sci.*, **184** [1–4] 393–8 (2001).

[3]H. Matsunami, "Current SiC Technology for Power Electronic Devices Beyond Si," *Microelectron. Eng.*, **83** [1] 2–4 (2006).

[4]K. Shenai, R. S. Scott, and B. J. Baliga, "Optimum Semiconductors for High-Power Electronics," *IEEE Trans. Electron Devices*, **36** [9] 1811–23 (1989).

[5]M. Bhatnagar and B. J. Baliga, "Comparison of 6H-SiC, 3C-SiC, and Si for Power Devices," *IEEE Trans. Electron Devices*, **40** [3] 645–55 (1993).

[6]B. Tang, S. R. Zhang, X. H. Zhou, Y. Yuan, and L. B. Yang, "Preparation and Modification of High Curie Point $BaTiO_3$-Based X9R Ceramics," *J. Electroceram.*, **25** [1] 93–7 (2010).

[7]J. Yamamatsu, N. Kawano, T. Arashi, A. Sato, Y. Nakano, and T. Nomura, "Reliability of Multilayer Ceramic Capacitors with Nickel Electrodes," *J. Power Sources*, **60** [2] 199–203 (1996).

[8]M.-J. Pan and C. A. Randall, "A Brief Introduction to Ceramic Capacitors," *IEEE Electr. Insul. Mag.*, **26** [3] 44–50 (2010).

[9]X. Xilin, A. S. Gurav, P. M. Lessner, and C. A. Randall, "Robust BME Class-I MLCCs for Harsh-Environment Applications," *IEEE Trans. Ind. Electron*, **58** [7] 2636–43 (2011).

[10]C. A. Randall, et al., "Improved Reliability Predictions in High Permittivity Dielectric Oxide Capacitors Under High dc Electric Fields with Oxygen Vacancy Induced Electromigration," *J. Appl. Phys.*, **113** [1] 014101, 6pp (2013).

[11]K. Kobayashi, M. Ryu, Y. Doshida, Y. Mizuno, and C. A. Randall, "Novel High- Temperature Antiferroelectric-Based Dielectric $NaNbO_3$–$NaTaO_3$ Solid Solutions Processed in Low Oxygen Partial Pressures," *J. Am. Ceram. Soc.*, **96** [2] 531–7 (2013).

[12]M. Acosta, J. Zang, W. Jo, and J. Rödel, "High-Temperature Dielectrics in $CaZrO_3$- Modified $Bi_{1/2}Na_{1/2}TiO_3$-Based Lead-Free Ceramics," *J. Eur. Ceram. Soc.*, **32** [16] 4327–34 (2012).

[13]Y. Yuan, S. R. Zhang, X. H. Zhou, B. Tang, and B. Li, "High-Temperature Capacitor Materials Based on Modified $BaTiO_3$," *J. Electron. Mater.*, **38** [5] 706–10 (2009).

[14]C.-C. Huang and D. P. Cann, "Phase Transitions and Dielectric Properties in $Bi(Zn_{1/2}Ti_{1/2})O_3$–$BaTiO_3$ Perovskite Solid Solutions," *J. Appl. Phys.*, **104** [2] 024117, 4pp (2008).

[15]H. Ogihara, C. A. Randall, and S. Trolier-McKinstry, "High-Energy Density Capacitors Utilizing $0.7BaTiO_3$–$0.3BiScO_3$ Ceramics," *J. Am. Ceram. Soc.*, **92** [8] 1719–24 (2009).

[16]H. Ogihara, C. A. Randall, and S. Trolier-McKinstry, "Weakly Coupled Relaxor Behavior of $BaTiO_3$–$BiScO_3$ Ceramics," *J. Am. Ceram. Soc.*, **92** [1] 110–8 (2009).

[17]J. Lim, S. Zhang, and T. Shrout, "High Temperature Capacitors Using a $BiScO_3$-$BaTiO_3$- $(K_{1/2}Bi_{1/2})TiO_3$ Ternary System," *Electron. Mater. Lett.*, **7** [1] 71–5 (2011).

[18]R. Dittmer, W. Jo, D. Damjanovic, and J. Rodel, "Lead-Free High-Temperature Dielectrics with Wide Operational Range," *J. Appl. Phys.*, **109** [3] 034107, 5 pp (2011).

[19]R. Dittmer, et al., "A High-Temperature-Capacitor Dielectric Based on $K_{0.5}Na_{0.5}NbO_3$-Modified $Bi_{1/2}Na_{1/2}TiO_3$–$Bi_{1/2}K_{1/2}TiO_3$," *J. Am. Ceram. Soc.*, **95** [11] 3519–24 (2012).

[20]N. Raengthon, T. Sebastian, D. Cumming, I. M. Reaney, and D. P. Cann, "$BaTiO_3$– $Bi(Zn_{1/2}Ti_{1/2})O_3$–$BiScO_3$ Ceramics for High-Temperature Capacitor Applications," *J. Am. Ceram. Soc.*, **95** [11] 3554–61 (2012).

[21]N. Raengthon and D. Cann, "High Temperature Electronic Properties of $BaTiO_3$–$Bi(Zn_{1/2}Ti_{1/2})O_3$–$BiInO_3$ for Capacitor Applications," *J. Electroceram.*, **28** [2–3] 165–71 (2012).

[22]W. Krauss, D. Schütz, M. Naderer, D. Orosel, and K. Reichmann, "BNT-Based Multilayer Device with Large and Temperature Independent Strain Made by a Water-Based Preparation Process," *J. Eur. Ceram. Soc.*, **31** [9] 1857–60 (2011).

[23]E. Sapper, A. Gassmann, L. Gjødvad, W. Jo, T. Granzow, and J. Rödel, "Cycling Stability of Lead-Free BNT–8BT and BNT–6BT–3KNN Multilayer Actuators and Bulk Ceramics," *J. Eur. Ceram. Soc.*, **34** [3] 653–61 (2014).

[24]I. Karakaya and W. T. Thompson, "The Ag−Pd (Silver-Palladium) System," *Bull. Alloy Phase Diagrams*, **9** [3] 237–43 (1988).

[25]S. F. Wang and W. Huebner, "Interaction of Silver/Palladium Electrodes with Lead-and Bismuth-Based Electroceramics," *J. Am. Ceram. Soc.*, **76** [2] 474–80 (1993).

[26]H. Nagata, K. Tabuchi, and T. Takenaka, "Fabrication and Electrical Properties of Multilayer Ceramic Actuator Using Lead-Free $(Bi_{1/2}K_{1/2})TiO_3$," *Jpn. J. Appl. Phys.*, **52** [9S1] 09KD05 (2013).

[27]D. Hennings, "Liquid Phase Sintering of Barium Titanate," *Berichte der Deutschen Keramischen Gesellschaft*, **55** [7] 359–60 (1978).

[28]H. Y. Tian, K. W. Kwok, H. L. W. Chan, and C. E. Buckley, "The Effects of CuO-Doping on Dielectric and Piezoelectric Properties of $Bi_{0.5}Na_{0.5}TiO_3$–$Ba(Zr,Ti)O_3$ Lead-Free Ceramics," *J. Mater. Sci.*, **42** [23] 9750–5 (2007).

[29]M. Matsubara, T. Yamaguchi, W. Sakamoto, K. Kikuta, T. Yogo, and S.-I. Hirano, "Processing and Piezoelectric Properties of Lead-Free (K,Na)$(Nb,Ta)O_3$ Ceramics," *J. Am. Ceram. Soc.*, **88** [5] 1190–6 (2005).

[30]E. Li, H. Kakemoto, S. Wada, and T. Tsurumi, "Influence of CuO on the Structure and Piezoelectric Properties of the Alkaline Niobate-Based Lead-Free Ceramics," *J. Am. Ceram. Soc.*, **90** [6] 1787–91 (2007).

[31]M. Ehmke, J. Glaum, W. Jo, T. Granzow, and J. Rödel, "Stabilization of the Fatigue- Resistant Phase by CuO Addition in $(Bi_{1/2}Na_{1/2})TiO_3$–$BaTiO_3$," *J. Am. Ceram. Soc.*, **94** [8] 2473–8 (2011).

[32]W. Jo, et al., "CuO as a Sintering Additive for $(Bi_{1/2}Na_{1/2})TiO_3$–$BaTiO_3$–$(K_{0.5}Na_{0.5})NbO_3$ Lead-Free Piezoceramics," *J. Eur. Ceram. Soc.*, **31** [12] 2107–17 (2011).

[33]H.-Y. Park, et al., "Low-Temperature Sintering and Piezoelectric Properties of CuO-Added $0.95(Na_{0.5}K_{0.5})NbO_3$–$0.05BaTiO_3$ Ceramics," *J. Am. Ceram. Soc.*, **90** [12] 4066–9 (2007).

[34]L. Dunmin, K. W. Kwok, and H. L. W. Chan, "Piezoelectric and Ferroelectric Properties of Cu-Doped $K_{0.5}Na_{0.5}NbO_3$ Lead-Free Ceramics," *J. Phys. D: Appl. Phys.*, **41** [4] 045401, 6pp (2008). □